

Surface Wettability Effect on Energy Density and Power Density of Supercapacitors

Shuangliang Zhao, Zhiying Song, Leying Qing, Jingmin Zhou, and Chongzhi Qiao*

Cite This: *J. Phys. Chem. C* 2022, 126, 9248–9256

Read Online

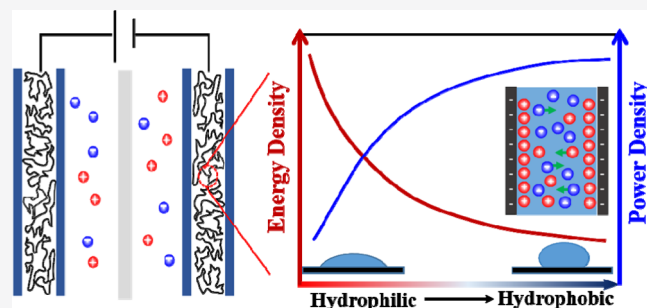
ACCESS |

Metrics & More

Article Recommendations

Supporting Information

ABSTRACT: Many attempts have been made to improve the energy density of supercapacitors toward their large-scale applications in storing renewable energy. Herein, the surface wettability effect is unraveled with the combination of static and dynamic density functional theories through which the energy densities and power densities of electrochemical supercapacitors are analyzed with different sets of pore sizes, surface voltages, and bulk ion concentrations. We demonstrate that tuning the surface wettability of electrodes may improve the energy density but simultaneously reduce the power density, and an optimal energy density with a relatively small cost of power density can be achieved by adopting highly confined pores. In addition, increasing ion bulk concentration and/or surface voltage can enhance both the energy density and power density. This work provides a complementary dynamic insight into the surface wettability effect on the performance of supercapacitors.



1. INTRODUCTION

Due to the urgent demands for environmental protection and CO₂ emission reduction, renewable energy plays a significant role in the future global energy portfolio.^{1–3} The extraction and energy storage of unstable green energy (i.e., solar energy, wind energy, and ocean energy) should be supported with energy storage systems for stabilizing the energy supply.^{4–6} The electric energy storage devices, including batteries, supercapacitors, and dielectric capacitors, have shown a growing potential,^{7,8} among which supercapacitors have attracted much attention for their merits of exceedingly high power density, long cycle life, safety, and environmentally friendly properties.^{9,10} However, supercapacitors generally have low energy density as they essentially rely on the physical adsorption of ions on the oppositely charged electrode surface, and this feature severely limits their large-scale applications.¹¹

Many experimental and theoretical attempts have been devoted to promoting the energy storage performance of supercapacitors by designing proper electrode materials and electrolyte solutions.^{12–14} The underlying idea lies in enhancing ion adsorption in microporous electrodes, which, in principle, can be achieved by increasing the specific surface area of the electrode and/or regulating the charge accumulation in the hierarchical pores of electrodes. For example, Zhang et al.¹⁵ demonstrated that a higher surface area and a smaller average pore diameter could significantly improve the capacitance of the supercapacitor. Using a template chemical vapor deposition (CVD) approach, Ning et al.¹⁶ prepared nanomesh graphene, and this new electrode material exhibited an excellent energy storage performance due to a high surface

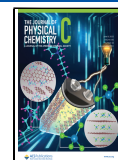
area. Chmiola et al.¹⁷ found that the capacitance anomalously increases when reducing the average pore size of the microporous electrodes down to 1 nm. It should be noted that the pore size effect is coupled with the sizes of charged molecules, and therefore, the ion desolvation in nanoscale pores can also significantly influence the supercapacitor performances.^{18,19}

The charge accumulation can also be regulated by manipulating the surface wettability (i.e., hydrophilicity or hydrophobicity) of the electrode material. Indeed, surface wettability can dramatically influence the distribution of the dielectric constant,^{20,21} which in turn affects the ion distribution near the electrode. Therefore, both theoretical and experimental attempts in past years have been made toward improving the capacitance of supercapacitors by tuning the surface wettability.^{20,22,23} Unfortunately, most of these studies focus solely on energy density, and the effect of surface wettability on power density is rarely explored. In other words, although the surface wettability not only affects the adsorption account of ions but also has great influence on the adsorption speed, the latter is associated with the adsorption dynamics on which the surface wettability effect is largely unknown. As a

Received: March 1, 2022

Revised: April 28, 2022

Published: May 25, 2022



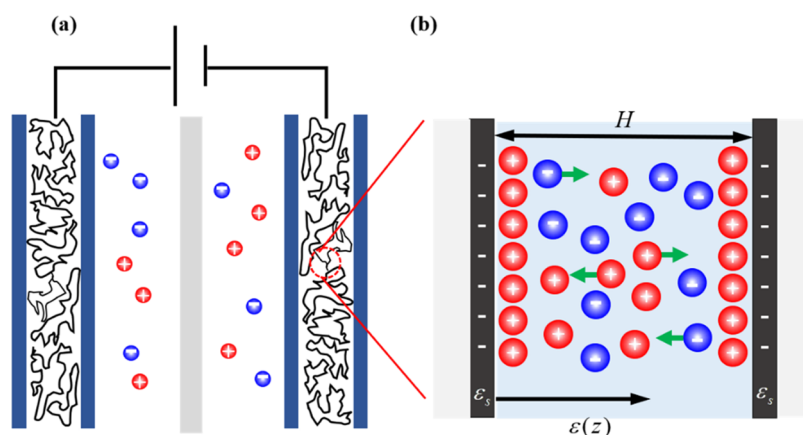


Figure 1. Schematic diagrams of the (a) supercapacitor with two electrodes and (b) representative slit pore from the porous anode.

matter of fact, most devices are operated under dynamic mode in practical applications, and the power density represents a key evaluator in the design of supercapacitors,^{24–26} and its variation against surface wettability should be carefully addressed.

In this work, both the static classical density functional theory (cDFT)²⁷ and dynamic density functional theory (DDFT) are employed to explore the surface wettability effect on the thermodynamic and dynamic properties of ion adsorption. cDFT represents an efficient tool to study the charge accumulation in electric double layer capacitors (EDLCs), which can well describe the molecular size effect and the interion electrostatic correlation.^{19,28,29} Derived from cDFT, DDFT is developed to study molecular diffusion including the ion adsorption dynamics during the charging/discharging process of EDLCs.^{30–32}

The remainder of this work is organized as follows. In Section 2, the model system is constructed, and the essential equations of DDFT and cDFT are introduced. In Section 3, the theoretical methods are validated by comparing the predictions with relevant simulation studies. Thereafter, the effects of surface wettability on both the energy density and power density are extensively analyzed and discussed. In addition, their coupling effects with pore size, surface voltage, and bulk ion concentration are addressed. Finally, a brief conclusion is given in Section 4.

2. MOLECULAR MODEL AND THEORY

2.1. Theoretical Model. The basic elements to a supercapacitor, in addition to the separator, are the two electrodes and the electrolyte between both electrodes as well as inside the hierarchical pores of porous electrodes, as illustrated in Figure 1a. Comparing with the area of the outer surface, the inner specific surface area of an electrode (usually the anode) caused by interconnected nanoscale pores is a few orders of magnitude larger. For example, a carbon-based anode possesses amazingly thousands of square meters per gram.³³ For ions adsorbed inside the numerous pores of an anode, the total adsorption amount can be determined by integrating the pore size distribution with the adsorption amount in each pore.²⁹ Therefore, the ion adsorption behavior in a single nanopore with a fixed pore size constitutes the cornerstone that needs to be comprehensively understood.

Toward this end, a structureless slit pore with pore width H is considered, and both walls of the slit pore are negatively

charged, which closely mimics a nanopore in the anode. Since the cation and anion have the same parameters and the same dielectric constant distribution, the density profile of the cation or anion near the cathode should be identical with the counterpart near the anode. In other words, the same conclusion holds if a positively charged wall is considered. We assume the pore length is much larger than the pore width so that the pore end effect can be neglected. As shown in Figure 1b, the electrolyte solution composed of explicit ions is confined inside the slit. The ions are described with the restricted primitive model (RPM) in which the cations and anions are described with hard spheres with identical diameter $\sigma_+ = \sigma_- = \sigma$, and they carry opposite charges $Z_i e$, where e is the elementary charge and Z_i is the valence of ion species ($i = +, -$). The walls of the slit are assumed to be hard walls with perfect conductivity, so that the electrostatic potential within each wall is constant. Hence, the wall–ion long-range interaction is solely composed of electrostatic interaction, and no dispersed interaction is included. In this work, we set $Z_+ = 1.0$ and $Z_- = -1.0$, and $\sigma = 0.425$ nm unless otherwise specified. The ion bulk density is ρ_i^b , corresponding to the bulk chemical potential μ_i^b . Due to the neutrality condition in the bulk system, we have $\rho_+^b = \rho_-^b$.

The electrolyte medium is assumed as a dielectric continuum. Since the surface wettability (hydrophobicity or hydrophilicity) changes the interfacial dielectric surroundings,^{34,35} and thus, the dielectric constant near a hydrophilic surface is generally higher than that near a hydrophobic one. For this reason, interfacial dielectric distribution has been utilized to characterize surface wettability.^{36–38} In the slit pore, the interfacial dielectric distribution varies along with the normal distance to the surface and can be designated as $\varepsilon(z)$, where z is the distance to the left charged surface (see Figure 1b). Following Podgornik et al.,³⁹ a simple yet efficient model is adopted

$$2\varepsilon(z) = \frac{\varepsilon_b}{1 + (\varepsilon_b/\varepsilon_s - 1)e^{-z/\lambda}} + \frac{\varepsilon_b}{1 + (\varepsilon_b/\varepsilon_s - 1)e^{-(H-z)/\lambda}} \quad (1)$$

where ε_s is the dielectric constant at the electrode surface and ε_b denotes the bulk dielectric constant. And λ is the microscopic parameter to scale the surface wettability. In this work, we set $\varepsilon_s = 10$ and $\varepsilon_b = 78.5$. In addition, as in a previous work,²⁰ we set $\lambda = 0.3$ nm for a hydrophilic surface, $\lambda = 0.9$ nm

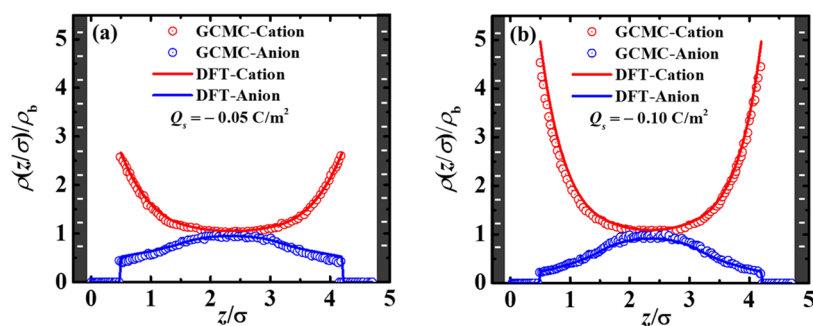


Figure 2. Comparison of normalized concentration distribution of ions $\rho_i(z/\sigma)/\rho_b$ from the DDFT calculation and GCMC simulation. The surface charge density at equilibrium state is (a) $Q_s = -0.05 \text{ C}\cdot\text{m}^{-2}$ and (b) $Q_s = -0.10 \text{ C}\cdot\text{m}^{-2}$.

for a neutrally wettable surface, and $\lambda = 1.5 \text{ nm}$ for a hydrophobic surface. The discussion between the microscopic parameter and the macroscopic contact angle is detailed below.

2.2. Dynamic Density Functional Theory. Physically, ion adsorption and diffusion are driven by the gradient of its local chemical potential $\mu_i(\mathbf{r}, t)$, and the latter quantity can be determined by the derivative of the Helmholtz free energy with respect to the local density of ions, viz., $\mu_i(\mathbf{r}, t) = \frac{\delta F[\{\rho_i(\mathbf{r}, t)\}]}{\delta \rho_i(\mathbf{r}, t)}$.

Within the framework of DDFT, the dynamical governing equation for the ion local density in the slit system follows⁴⁰

$$\frac{\partial \rho_i(z, t)}{\partial t} = \beta D \nabla \cdot \left[\rho_i(z, t) \nabla \frac{\delta F[\{\rho_i(z, t)\}]}{\delta \rho_i(z, t)} \right] \quad (2)$$

where D is the diffusion coefficient, which is assumed as a constant. And $\beta = 1/(k_B T)$ is defined by the Boltzmann constant k_B and system temperature T . The Helmholtz free energy functional within the DDFT framework is identical to that within cDFT⁴⁰ and it contains three contributions

$$F[\{\rho_i(\mathbf{r}, t)\}] = F^{\text{id}}[\{\rho_i(z, t)\}] + F^{\text{ex}}[\{\rho_i(z, t)\}] + \sum_i \int \rho_i(z, t) V_i^{\text{ext}}(z) \text{d}\mathbf{r} \quad (3)$$

The first term on the right-hand side accounts for the ideal gas contribution, and the second one accounts for the interactions among ions, which include the hard-sphere interaction and electrostatic interaction, and the calculation details are listed in the Supporting Information (SI). $V_i^{\text{ext}}(z)$ in the last term represents the external potential of the i th ion component originating from the wall–ion interaction.

Under the condition of thermodynamic equilibrium, the ion local density is irrelevant with time, viz., $\partial \rho_i / \partial t = 0$, and then the dynamical governing equation can be reduced to

$$\nabla \cdot \left[\rho_i(z, t) \nabla \frac{\delta \beta F[\{\rho_i(z, t)\}]}{\delta \rho_i(z, t)} \right] = 0 \quad (4)$$

As the confined system is connected with the electrolyte solution outside the anode (considered as a bulk reservoir), the ion local chemical potential inside the slit is constant everywhere at thermodynamic equilibrium and equals its counterpart in the bulk system, μ_i^b , and thus the above equation recovers to cDFT

$$\frac{\delta F[\rho_i(z)]}{\delta \rho_i(z)} = \mu_i^b \quad (5)$$

We note that the bulk chemical potential is conjugated with the ion bulk density, ρ_i^b . In other words, the bulk chemical potential μ_i^b (or the ion bulk density ρ_i^b) can be determined by the corresponding ion bulk density (or the bulk chemical potential) through the equation of state. As the same functional is applied in both DDFT and cDFT, the final equilibrium density profile predicted by DDFT should be identical to that from cDFT.⁴⁰

To describe the charging process, the surface charge density, Q_s , can be obtained by applying the charge neutrality condition when⁴¹

$$Q_s(t) = - \int_0^{H/2} \sum_i e Z_i \rho_i(z, t) \text{d}z \quad (6)$$

At thermodynamic equilibrium, the surface charge density reaches a constant value, designated as Q_s^e , and then the integral capacitance can be determined by

$$C = Q_s^e / V_s \quad (7)$$

where V_s is the applied surface voltage. Thereafter, the energy density, E , and the power density, P , can be determined by

$$\begin{cases} E = \frac{1}{2} C V_s^2 \\ P = \frac{E}{t_{\text{eq}}} \end{cases} \quad (8)$$

where t_{eq} is the charging duration time, and it can be determined through time evolution of surface charge density. Practically, when $Q_s(t)$ reaches 98% of Q_s^e , the time elapsed refers to the charging duration time.

At the initial state (i.e., charging time $t = 0$), the density profiles of cations and anions are computed using cDFT with a zero surface voltage and a uniform dielectric constant, $\epsilon = \epsilon_b$. Owing to the symmetry of the nonelectrostatic interaction from both pore walls, the density distributions of cations and anions confined in the slit pore are identical, i.e., $\rho_+(z, t = 0) = \rho_-(z, t = 0)$.

3. RESULTS AND DISCUSSION

3.1. Validation of Theoretical Calculation. The ion density distribution near the charged interface represents the primary quantity for evaluating the electrochemical properties. To verify the reliability of the theoretical calculation, we compare the equilibrium ion density distribution in a slit pore predicted by DDFT with relevant grand canonical Monte Carlo (GCMC) simulations.^{42,43} Figure 2 shows the

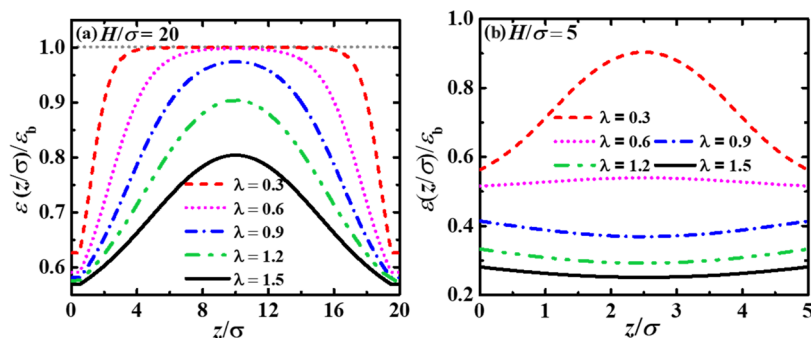


Figure 3. Normalized interfacial dielectric constant distributions $\varepsilon(z/\sigma)/\varepsilon_b$ in the two representative slit pores for five surface wetting parameters ($\lambda = 0.3, 0.6, 0.9, 1.2,$ and 1.5 nm): (a) $H/\sigma = 20$, $V_s = 0.3$ V, and $\rho_b\sigma^3 = 0.29$ and (b) $H/\sigma = 5$, $V_s = 0.03$ V, and $\rho_b\sigma^3 = 0.0462$.

normalized concentration distributions of co-ions and counterions from DDFT at the final equilibrium state and GCMC simulation at different surface charge densities. In this comparison, the RMP model of ion and wall–ion interaction is employed as described above. The system temperature, T , is 298 K, the width of the slit pore, H , is 20 Å, the ion size is set as $\sigma_+ = \sigma_- = \sigma = 0.425$ nm, and the bulk ion concentration, c_b , is equal to 1.0 M, corresponding to the reduced bulk density, $\rho_b\sigma^3 = (\rho_+^b + \rho_-^b)\sigma^3 = 2\rho_+^b\sigma^3 = 0.0462$. It should be mentioned that in both the simulation and DDFT calculations, the uniform dielectric constant $\varepsilon_b = 78.5$ is adopted for the electrolyte solution in the whole space.

At equilibrium state, the counterions compactly accumulate near the charged wall of the slit pore, subsequently distributing in the outer diffusion layer. Due to the electrostatic repulsion from both the charged walls and accumulated counterions, the co-ions are repelled away from the surfaces and mainly accumulate at the center of the slit pore. Additionally, the local density of the co-ion in whole space is overall lower than that of the counterion, and this is because both pore walls are negatively charged, and thus the adsorption amount of the cation is larger than the anion. The predicted ion local density distributions are in excellent agreement with the parallel simulation results, validating the accuracy of our DDFT calculation.

3.2. Surface Wettability Effect. We first discuss the relationship between the surface wetting parameter, λ , and the interfacial dielectric distribution, $\varepsilon(z)$. Figure 3 shows the interfacial dielectric distribution, $\varepsilon(z)$, in the slit pores with five typical surface wetting parameters, i.e., $\lambda = 0.3, 0.6, 0.9, 1.2,$ and 1.5 nm. Two typical pore sizes are considered including $H^* = H/\sigma = 20$ and 5.

For the system with a large pore size, as depicted in Figure 3a, the dielectric constant is small near both the surfaces, and gradually increases when enlarging the distance to the surface of the electrodes, and it approaches the bulk value when the interfacial effect vanishes. It is to be noted that a small dielectric constant distribution near the wall can decrease the ion density at the adsorption layer, which means that the small dielectric constant in the interfacial zone can mimic a hydrophilic wall, as mentioned in the previous work.²⁰ In addition, we note that a larger surface wetting parameter (thus, a more hydrophobic surface) leads to a stronger interfacial effect. When the surface wetting parameter is sufficiently large (i.e., $\lambda \geq 0.9$ nm), the dielectric constant at the center of the slit pore is still below the bulk value. This trend becomes even more prominent as $\lambda = 1.5$ nm. For the system with a small pore size as shown in Figure 3b, the wettability effects from

both walls may be overlapped at the center of the slit pore, and due to this overlapping, the dielectric constant is even smaller than the bulk value under the condition $\lambda \geq 0.9$ nm.

To further demonstrate the quantitative description of surface wettability, we explore the correlation between the wetting parameter and the surface contact angle, θ , in electrostatic fields. Virtually, several monotonous correspondence relations have been proposed for correlating both quantities. For instance, to investigate the influence of the applied electrostatic field on the contact angle, Verheijen et al.³⁶ proposed an electrowetting equation in which the relation between the dielectric constant and the contact angle is derived from the Lippmann equation by employing the parallel-capacitor approximation for the droplet–dielectric interface. The same relation is also reported by Kang³⁷ after considering the thermodynamic equilibrium condition as follows

$$\cos \theta = \cos \theta_0 + \frac{\varepsilon_d V_s^2}{2\gamma d} \quad (9)$$

where θ_0 is the contact angle without imposing an external electrostatic field, V_s is the applied surface voltage, γ is the surface tension, and d is the thickness of the dielectric layer. The dielectric constant ε_d is a position-independent constant. The above model can be extended by replacing the dielectric constant ε_d with the averaged value $\bar{\varepsilon}$ within the Stern layer. In other words, we assume $\varepsilon_d = \bar{\varepsilon}$, and the averaged dielectric constant, $\bar{\varepsilon}$, can be calculated through the interfacial dielectric distribution as

$$\bar{\varepsilon} = \frac{1}{\sigma} \int_0^\sigma \varepsilon(z) dz \quad (10)$$

Here, the thickness of the Stern layer has been assumed to be σ . To illustrate the response of the contact angle to the dielectric constant (hence the surface wetting parameter), we take the ionic fluid confined in a slit pore as a reference system. The thickness of the dielectric layer is 0.34 nm, and the initial contact angle for zero applied voltage, θ_0 , is assumed to be 75° , the surface tension, γ , is 59.1 mJ m⁻², and the surface voltage, V_s , is equal to 0.3 V. In this circumstance, the dependence of the contact angle on the surface wetting parameter is shown in Figure 4. It clearly indicates that the contact angle monotonously increases with the increase in surface wettability, and this confirms that increasing the wetting parameter can faithfully mimic the change of surface wettability from hydrophilicity to hydrophobicity. In addition, this change is more evident when the pore size is smaller.

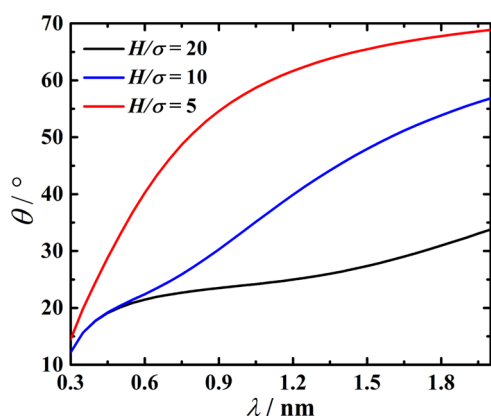


Figure 4. Change of contact angle, θ , with the surface wetting parameter, λ , for the ionic fluid confined in different slit pores.

Incorporated with the interfacial dielectric constant distribution, we thereafter study the effect of surface wettability on the dynamic charging process. Figure 5 shows the time evolution of the surface charge density with two typical surface wetting parameters, $\lambda = 0.3$ and 1.5 nm. The surface charge density is calculated through eq 6, and the time-dependent ionic density in the like-charged slit pore are calculated with DDFT. To explore the influences of the applied surface voltage, pore size, and ion bulk concentration, we attempt two applied surface voltages (i.e., $V_s = 0.03$ and 0.05 V), two pore sizes (i.e., $H/\sigma = 5$ and 10), and two ion bulk concentrations (i.e., $c_b = 1.0$ and 1.3 M). We observe a typical behavior during the charging process in that the surface charge density generally increases over time and reaches a final plateau. The plateau is higher when the surface voltage is larger or the ion bulk concentration is higher. The pore size has little effect on the plateau when the surface wetting parameter is small. However, when the surface wetting parameter is large (for example, $\lambda = 1.5$ nm), the surface wettability effects from both pore walls are overlapped in the slit pores with pore size $H/\sigma = 5$ and 10 , as discussed in Figure 3, and then the pore size has a prominent effect on the plateau. Indeed, when the pore is smaller, the surface wettability effects from both pore walls on the confined ionic fluid become relatively stronger, and hence the surface charge density plateau is suppressed. This trend is consistent with the analysis on the variation of wetting parameters.

By comparing the curves of same color in Figure 5a,b, we find that increasing the wetting parameter can suppress the plateau value of the surface charge density. In addition, we

note that there is a peak in the blue or pink curve in Figure 5b, indicating that there is a “turn-over” point in the surface charge density. This turn-over phenomenon has been reported by many works,³¹ and it is mainly attributed to the inhomogeneous distribution of dielectric constant.⁴⁴

Next, the effect of surface wettability on the capacitance is examined. Figure 6a presents the capacitance of the charged slit pore with pore width of $H/\sigma = 2$. The capacitance decreases first and then flattens out with the increase of λ , showing that the hydrophilic surface is beneficial to improving the capacitance, being consistent with the experimental results.¹⁶ When the ion bulk density remains constant, the increase in the surface voltage promotes the capacitance significantly. Specifically, when increasing the surface voltage from 0.01 to 0.05 V, the capacitance increases almost 4-fold. However, variation in the ion bulk density brings little effect on the capacitance. In Figure 6b, the charged slit with a large pore width of $H/\sigma = 5$ is considered. The capacitance decreases linearly with increasing surface wetting parameter from 0.3 to 1.5 nm. Compared with Figure 6a, although the variation in the applied voltage has less influence on the capacitance, the effect of ion bulk density is more prominent, and in addition, the surface wettability plays a more significant role in the capacitance.

Next, the effects of surface wettability on the energy storage capacity and charging rate are examined. The energy density and power density are calculated through eq 8. As shown in Figure 7a,b, with the increase of the surface wetting parameter λ , the energy density decreases monotonically, while the power density increases overall and gradually approaches a plateau. As discussed above, the hydrophilic surface can adsorb more net charge, thus bringing larger capacitance and energy storage. The hydrophilic surface presents a strong attractive interaction with water molecules, hence significantly promoting the water density in the vicinity of the wall. The high density causes close spatial packing of the water molecule, hindering the ions from moving to the wall. Therefore, it takes a longer time to accomplish the charging process as shown in Figure 5a, which results in a smaller power density. In the slit pore with $H/\sigma = 2$, when increasing the surface wetting parameter from 0.3 to 1.5 nm, the energy density decreases by 60%, while the power density increases by 14%. However, in the slit pore with $H/\sigma = 5$, the energy density decreases by 48%, while the power density increases by 53%. Comparison between both the cases shows that the hydrophilic material as electrode is more beneficial for promoting energy storage, but inevitably results in the descent of power density. In addition, the surface

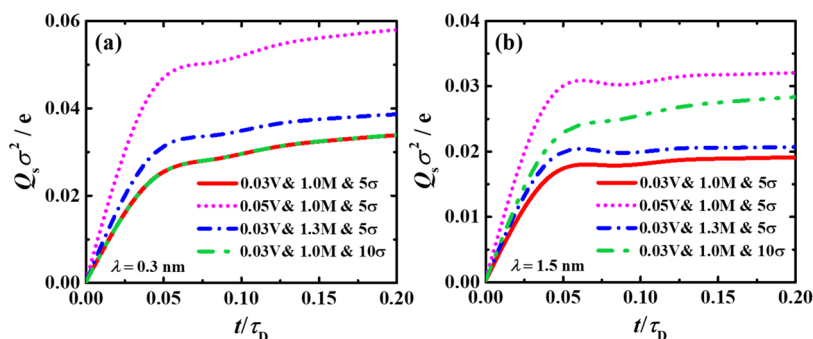


Figure 5. Change of the surface charge density with time under different conditions: (a) $\lambda = 0.3$ nm represents a hydrophilic surface and (b) $\lambda = 1.5$ nm represents a hydrophobic surface.

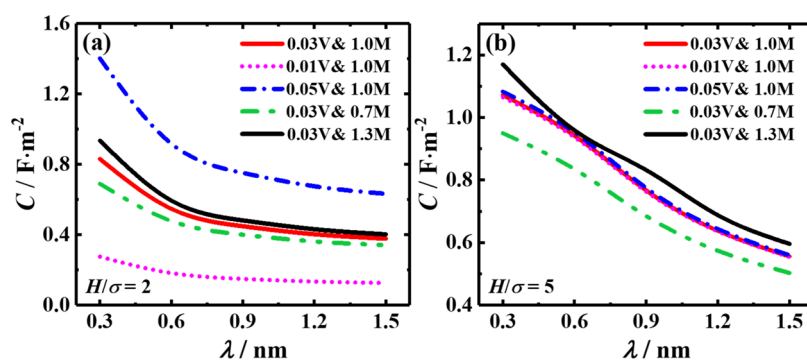


Figure 6. Capacitance against the surface wetting parameter under different conditions: (a) $H/\sigma = 2$ and (b) $H/\sigma = 5$.

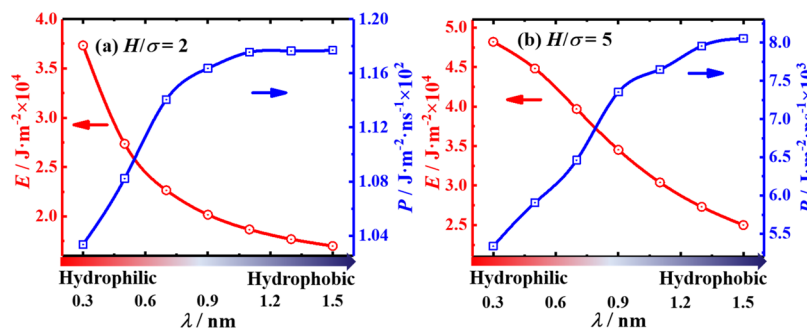


Figure 7. Energy density and power density against the surface wetting parameter λ . The system parameters are (a) $H/\sigma = 2$, $V_s = 0.03$ V, and $\rho_b\sigma^3 = 0.0462$ and (b) $H/\sigma = 5$, $V_s = 0.03$ V, and $\rho_b\sigma^3 = 0.0462$.

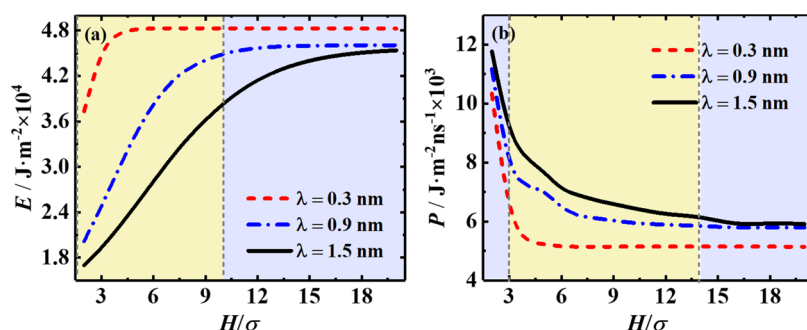


Figure 8. (a) Energy density and (b) power density as a function of the pore size H/σ at three surface wetting parameters: $\lambda = 0.3, 0.9,$ and 1.5 nm. The surface voltage is $V_s = 0.03$ V and the ion bulk density is $\rho_b\sigma^3 = 0.0462$.

wettability effect is more significant in smaller pores on energy density and in larger pores on power density.

3.3. Regulating Energy Density and Power Density.

As both the energy density and power density can be influenced by the pore size, applied surface voltage, and ion bulk density in the electrolyte solution, below, we evaluate the wettability effects under different conditions.

Figure 8a,b shows the energy density and power density varying with the pore size. Three surface wetting parameters, $\lambda = 0.3, 0.9,$ and 1.5 nm are studied, corresponding to the hydrophilic surface, neutrally wettable surface, and hydrophobic surface. The energy density first increases with the increase of H/σ at small H/σ , where the cations and anions can be completely separated due to the strong overlapping effect of the electrostatic potential. As the pore size H/σ further increases, the energy density approaches a plateau due to the saturation of the stored charges near the electrode surface.

Herein, we introduce a factor to quantify the effect of wettability

$$\alpha = \frac{|X(\lambda = 1.5) - X(\lambda = 0.3)|}{\max\{X(\lambda = 1.5), X(\lambda = 0.3)\}} \quad (11)$$

where X represents a physical quantity that depends on wettability, i.e., energy density and power density. Based on factor α , Figure 8a,b can be divided into two zones, the yellow zones ($\alpha > 20\%$) and the blue zones ($\alpha \leq 20\%$), which signify the areas denoting the significant surface wettability effect and negligible surface wettability effect, respectively. For energy density, the wettability effect can be ignored with a pore size $H/\sigma > 10$, as shown in Figure 8a. Figure 8b shows that the wettability can considerably affect the power density with the pore size H/σ varying between 3 and 14. Therefore, it can be found that when the pore size $H/\sigma = 10-14$, the surface wettability has little influence on energy density but significant influence on power density. In contrast, when the pore size $H/\sigma = 1-3$, the surface wettability has a significant influence on energy density but little influence on power density.

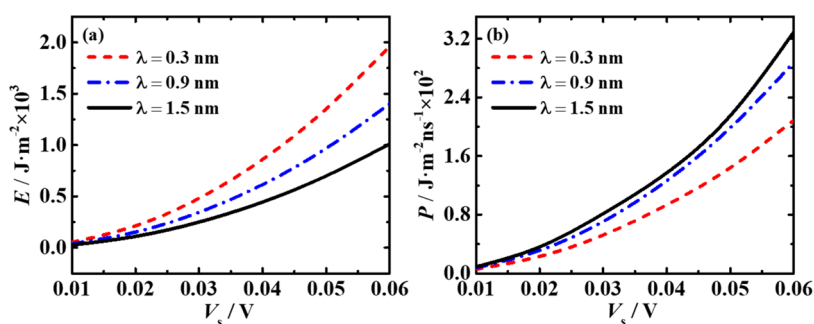


Figure 9. (a) Energy density and (b) power density in terms of surface voltage at three types of surface wettability, i.e., $\lambda = 0.3, 0.9$, or 1.5 nm. The pore size is fixed at $H/\sigma = 5$ and the ion bulk density is $\rho_b\sigma^3 = 0.0462$.

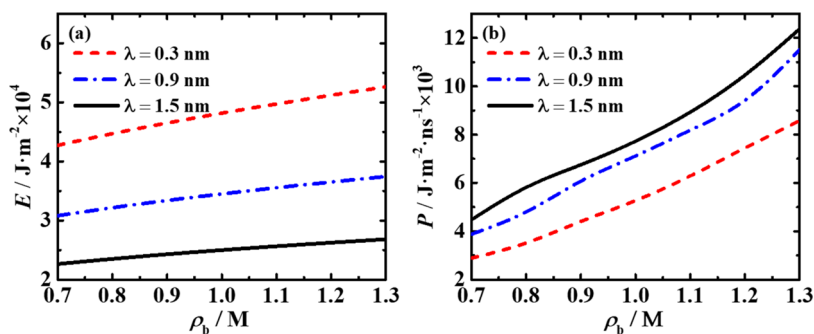


Figure 10. (a) Energy density and (b) power density varying with ion bulk density at three types of surface wettability, $\lambda = 0.3, 0.9$, or 1.5 nm. The pore size is $H/\sigma = 5$ and the surface voltage is $V_s = 0.03$ V.

Figure 9a,b shows the variations of energy density and power density against the applied surface voltages at three types of surface wettability, i.e., $\lambda = 0.3, 0.9$ and 1.5 nm. First, the increase in the surface voltage leads to the rise of both the energy density and power density. Second, the surface wettability effect on both energy density and power density becomes more and more significant when increasing the surface voltage. Especially, when the applied voltage is 0.06 V, the energy density is $2.0 \times 10^3 \text{ J} \cdot \text{m}^{-2}$ for $\lambda = 0.3$ nm and $1.0 \times 10^3 \text{ J} \cdot \text{m}^{-2}$ for $\lambda = 1.5$ nm, and the power density is $2.0 \times 10^2 \text{ J} \cdot \text{m}^{-2} \cdot \text{ns}^{-1}$ for $\lambda = 0.3$ nm and $3.2 \times 10^2 \text{ J} \cdot \text{m}^{-2} \cdot \text{ns}^{-1}$ for $\lambda = 1.5$ nm. This means the energy density can increase by 100%, while the power density can decrease by 40% by increasing the surface wettability at a high surface voltage.

Figure 10a,b shows the energy density and power density varying with the ion bulk density at three surface wetting parameters, $\lambda = 0.3, 0.9$, and 1.5 nm. Both the energy density and power density increase with the augment of the ion bulk density. In addition, this effect is more significant for the power density. In particular, when the ion bulk density changes from 0.7 to 1.3 M, the energy density increases by about 20%, while the power density increases by nearly 200%. This shows that the power density is more sensitive to the variation of ion bulk density. Indeed, when more ions are included, the ion diffusion is greatly accelerated due to the strong electrostatic interaction, and the time taken for the system to reach equilibrium is much reduced.

4. CONCLUSIONS

In this work, the effects of surface wettability on both the energy density and power density are evaluated by combining cDFT and DDFT. These effects are systematically assessed in a single like-charged slit pore system under different conditions

by varying the pore size, surface voltage, and ion bulk concentration.

We find that increasing the surface wettability can generally promote the energy density, but meanwhile suppress the power density, and the surface wettability effect is more significant on energy density in smaller pores and on power density in larger pores. Increasing the surface voltage and/or ion bulk concentration can simultaneously improve both the energy density and power density, and in addition, the power density is more sensitive to the variation in the surface voltage and ion bulk density. Further, by quantifying the surface wettability effect varying with pore width, we find that in highly confined pores with pore size $H/\sigma = 1-3$, the surface wettability has little influence on energy density but significant influence on power density. Here, we should mention that the diffusion coefficient of ions, in principle, depends on the ion local density.^{45,46} The pore size^{47,48} and surface hydrophilicity^{49,50} can affect the ion's density profile near the wall and further influence the diffusion coefficient. However, in the present study, the ion concentration is rather low, and thus we follow previous works^{20,28,41,44} and simply assume that the diffusion coefficient is a position-independent constant.

In short, these results suggest that the surface wettability effects on both thermodynamical and dynamical properties should be taken into account in the electrode material design, and an optimal energy density with a relatively small cost of power density can be achieved by adopting highly confined hydrophilic pores with large surface voltages and high ion bulk concentration.

■ ASSOCIATED CONTENT

Supporting Information

The Supporting Information is available free of charge at <https://pubs.acs.org/doi/10.1021/acs.jpcc.2c01455>.

Evaluation of Helmholtz free energy functional and numerical calculation details of DDFT (PDF)

AUTHOR INFORMATION

Corresponding Author

Chongzhi Qiao – State Key Laboratory of Chemical Engineering and School of Chemical Engineering, East China University of Science and Technology, Shanghai 200237, China; orcid.org/0000-0003-1132-5997; Email: czqiao@ecust.edu.cn

Authors

Shuangliang Zhao – State Key Laboratory of Chemical Engineering and School of Chemical Engineering, East China University of Science and Technology, Shanghai 200237, China; Guangxi Key Laboratory of Petrochemical Resource Processing and Process Intensification Technology and School of Chemistry and Chemical Engineering, Guangxi University, Nanning 530004, China; orcid.org/0000-0002-9547-4860

Zhiying Song – State Key Laboratory of Chemical Engineering and School of Chemical Engineering, East China University of Science and Technology, Shanghai 200237, China

Leying Qing – State Key Laboratory of Chemical Engineering and School of Chemical Engineering, East China University of Science and Technology, Shanghai 200237, China

Jingmin Zhou – Guangxi Key Laboratory of Petrochemical Resource Processing and Process Intensification Technology and School of Chemistry and Chemical Engineering, Guangxi University, Nanning 530004, China

Complete contact information is available at:
<https://pubs.acs.org/10.1021/acs.jpcc.2c01455>

Notes

The authors declare no competing financial interest.

ACKNOWLEDGMENTS

This work is supported by the National Natural Science Foundation of China (Nos. 22008063 and 21878078), and the Dean Project of Guangxi Key Laboratory of Petrochemical Resource Processing and Process Intensification Technology (No. 2020Z002).

REFERENCES

- (1) Sastry, S. V. A. R.; Sreenu, P. In *New Energy Sources and Its Sustainability*, 2012 IEEE International Conference on Engineering Education: Innovative Practices and Future Trends (AICERA); IEEE, 2012; pp 1–15.
- (2) Chu, S.; Majumdar, A. Opportunities and Challenges for a Sustainable Energy Future. *Nature* **2012**, *488*, 294–303.
- (3) Yip, N. Y.; Brogioli, D.; Hamelers, H. V. M.; Nijmeijer, K. Salinity Gradients for Sustainable Energy: Primer, Progress, and Prospects. *Environ. Sci. Technol.* **2016**, *50*, 12072–12094.
- (4) Zhan, C.; Lian, C.; Zhang, Y.; Thompson, M. W.; Xie, Y.; Wu, J.; Kent, P. R. C.; Cummings, P. T.; Jiang, D.; Wesolowski, D. J. Computational Insights into Materials and Interfaces for Capacitive Energy Storage. *Adv. Sci.* **2017**, *4*, No. 1700059.
- (5) Osti, N. C.; Dyatkin, B.; Thompson, M. W.; Tiet, F.; Zhang, P.; Dai, S.; Tyagi, M.; Cummings, P. T.; Gogotsi, Y.; Wesolowski, D. J.; Mamontov, E. Influence of Humidity on Performance and Microscopic Dynamics of an Ionic Liquid in Supercapacitor. *Phys. Rev. Mater.* **2017**, *1*, No. 035402.
- (6) Van Voorden, A. M.; Ramirez Elizondo, L. M.; Paap, G. C.; Verboomen, J.; Van Der Sluis, L. In *The Application of Super*

Capacitors to Relieve Battery-Storage Systems in Autonomous Renewable Energy Systems, 2007 IEEE Lausanne Power Tech; IEEE, 2007; pp 479–484.

(7) Zhong, C.; Deng, Y.; Hu, W.; Qiao, J.; Zhang, L.; Zhang, J. A Review of Electrolyte Materials and Compositions for Electrochemical Supercapacitors. *Chem. Soc. Rev.* **2015**, *44*, 7484–7539.

(8) Vlcek, L.; Zhang, Z.; Machesky, M. L.; Fenter, P.; Rosenqvist, J.; Wesolowski, D. J.; Anovitz, L. M.; Predota, M.; Cummings, P. T. Electric Double Layer at Metal Oxide Surfaces: Static Properties of the Cassiterite-Water Interface. *Langmuir* **2007**, *23*, 4925–4937.

(9) Voukadinova, A.; Gillespie, D. Energetics of Counterion Adsorption in the Electrical Double Layer. *J. Chem. Phys.* **2019**, *150*, No. 154706.

(10) Zhang, Y.; Cummings, P. T. Effects of Solvent Concentration on the Performance of Ionic-Liquid/Carbon Supercapacitors. *ACS Appl. Mater. Interfaces* **2019**, *11*, 42680–42689.

(11) Xing, L.; Vatamanu, J.; Smith, G. D.; Bedrov, D. Nanopatterning of Electrode Surfaces as a Potential Route to Improve the Energy Density of Electric Double-Layer Capacitors: Insight from Molecular Simulations. *J. Phys. Chem. Lett.* **2012**, *3*, 1124–1129.

(12) Van Aken, K. L.; Beidaghi, M.; Gogotsi, Y. Formulation of Ionic-Liquid Electrolyte To Expand the Voltage Window of Supercapacitors. *Angew. Chem.* **2015**, *127*, 4888–4891.

(13) Jana, M.; Khanra, P.; Murmu, N. C.; Samanta, P.; Lee, J. H.; Kuila, T. Covalent Surface Modification of Chemically Derived Graphene and Its Application as Supercapacitor Electrode Material. *Phys. Chem. Chem. Phys.* **2014**, *16*, 7618–7626.

(14) Da, Y.; Liu, J.; Zhou, L.; Zhu, X.; Chen, X.; Fu, L. Engineering 2D Architectures toward High-Performance Micro-Supercapacitors. *Adv. Mater.* **2019**, *31*, No. 1802793.

(15) Zhang, X.; Shi, W.; Zhu, J.; Zhao, W.; Ma, J.; Mhaisalkar, S.; Maria, T. L.; Yang, Y.; Zhang, H.; Hng, H. H.; Yan, Q. Synthesis of Porous NiO Nanocrystals with Controllable Surface Area and Their Application as Supercapacitor Electrodes. *Nano Res.* **2010**, *3*, 643–652.

(16) Ning, G.; Fan, Z.; Wang, G.; Gao, J.; Qian, W.; Wei, F. Gram-Scale Synthesis of Nanomesh Graphene with High Surface Area and Its Application in Supercapacitor Electrodes. *Chem. Commun.* **2011**, *47*, 5976–5978.

(17) Chmiola, J.; Yushin, G.; Gogotsi, Y.; Portet, C.; Simon, P.; Taberna, P.-L. Anomalous increase in carbon capacitance at pore sizes less than 1 nanometer. *Science* **2006**, *313*, 1760–1763.

(18) Largeot, C.; Portet, C.; Chmiola, J.; Taberna, P. L.; Gogotsi, Y.; Simon, P. Relation between the Ion Size and Pore Size for an Electric Double-Layer Capacitor. *J. Am. Chem. Soc.* **2008**, *130*, 2730–2731.

(19) Qing, L.; Tao, J.; Yu, H.; Jiang, P.; Qiao, C.; Zhao, S.; Liu, H. A Molecular Model for Ion Dehydration in Confined Water. *AIChE J.* **2020**, *66*, No. e16938.

(20) Ma, M.; Zhao, S.; Liu, H.; Xu, Z. Microscopic Insights into the Efficiency of Capacitive Mixing Process. *AIChE J.* **2017**, *63*, 1785–1791.

(21) Fan, Z.; Wang, Y.; Xie, Z.; Wang, D.; Yuan, Y.; Kang, H.; Su, B.; Cheng, Z.; Liu, Y. Modified MXene/Holey Graphene Films for Advanced Supercapacitor Electrodes with Superior Energy Storage. *Adv. Sci.* **2018**, *5*, No. 1800750.

(22) Liu, T.; Wang, K.; Chen, Y.; Zhao, S.; Han, Y. Dominant Role of Wettability in Improving the Specific Capacitance. *Green Energy Environ.* **2019**, *4*, 171–179.

(23) Avasthi, P.; Balakrishnan, V. Tuning the Wettability of Vertically Aligned CNT–TiO₂ Hybrid Electrodes for Enhanced Supercapacitor Performance. *Adv. Mater. Interfaces* **2019**, *6*, No. 1801842.

(24) Burt, R.; Birkett, G.; Zhao, X. S. A Review of Molecular Modelling of Electric Double Layer Capacitors. *Phys. Chem. Chem. Phys.* **2014**, *16*, 6519–6538.

(25) Lian, C.; Liu, H.; Li, C.; Wu, J. Hunting Ionic Liquids with Large Electrochemical Potential Windows. *AIChE J.* **2019**, *65*, 804–810.

- (26) Lian, C.; Janssen, M.; Liu, H.; van Roij, R. Blessing and Curse: How a Supercapacitor's Large Capacitance Causes Its Slow Charging. *Phys. Rev. Lett.* **2020**, *124*, No. 076001.
- (27) Wu, J.; Li, Z. Density-Functional Theory for Complex Fluids. *Annu. Rev. Phys. Chem.* **2007**, *58*, 85–112.
- (28) Lian, C.; Zhao, S.; Liu, H.; Wu, J. Time-Dependent Density Functional Theory for the Charging Kinetics of Electric Double Layer Containing Room-Temperature Ionic Liquids. *J. Chem. Phys.* **2016**, *145*, No. 204707.
- (29) Qing, L.; Long, T.; Yu, H.; Li, Y.; Tang, W.; Bao, B.; Zhao, S. Quantifying Ion Desolvation Effects on Capacitances of Nanoporous Electrodes with Liquid Electrolytes. *Chem. Eng. Sci.* **2021**, *240*, No. 116662.
- (30) Jiang, J.; Cao, D.; Jiang, D.; Wu, J. Kinetic Charging Inversion in Ionic Liquid Electric Double Layers. *J. Phys. Chem. Lett.* **2014**, *5*, 2195–2200.
- (31) Gao, H.; Xiao, C. Viscosity Effects for Ion Transport in Electrochemical Systems. *Europhysics Lett.* **2018**, *124*, No. 58002.
- (32) Liu, Y.; Liu, H. Time-Dependent Density Functional Theory for Fluid Diffusion in Graphene Oxide Membranes/Graphene Membranes. *Chem. Eng. Sci.* **2018**, *188*, 150–157.
- (33) Vlad, A.; Balducci, A. Supercapacitors: Porous Materials Get Energized. *Nat. Mater.* **2017**, *16*, 161–162.
- (34) Zhao, S.; Hu, Y.; Yu, X.; Liu, Y.; Bai, Z.-S.; Liu, H. Surface Wettability Effect on Fluid Transport in Nanoscale Slit Pores. *AIChE J.* **2017**, *63*, 1704–1714.
- (35) Bonthuis, D. J.; Gekle, S.; Netz, R. R. Dielectric Profile of Interfacial Water and Its Effect on Double-Layer Capacitance. *Phys. Rev. Lett.* **2011**, *107*, No. 166102.
- (36) Verheijen, H. J. J.; Prins, M. W. J. Reversible Electrowetting and Trapping of Charge: Model and Experiments. *Langmuir* **1999**, *15*, 6616–6620.
- (37) Kang, K. H. How Electrostatic Fields Change Contact Angle in Electrowetting. *Langmuir* **2002**, *18*, 10318–10322.
- (38) Karnik, R.; Fan, R.; Yue, M.; Li, D.; Yang, P.; Majumdar, A. Electrostatic Control of Ions and Molecules in Nanofluidic Transistors. *Nano Lett.* **2005**, *5*, 943–948.
- (39) Podgornik, R.; Cevc, G.; Žekš, B. Solvent Structure Effects in the Macroscopic Theory of van Der Waals Forces. *J. Chem. Phys.* **1987**, *87*, 5957–5967.
- (40) Qiao, C.; Zhao, T.; Yu, X.; Qing, L.; Bao, B.; Zhao, S.; Liu, H. On the Relation between Dynamical Density Functional Theory and Navier-Stokes Equation. *Chem. Eng. Sci.* **2021**, *230*, No. 116203.
- (41) Qing, L.; Zhao, S.; Wang, Z.-G. Surface Charge Density in Electrical Double Layer Capacitors with Nanoscale Cathode–Anode Separation. *J. Phys. Chem. B* **2021**, *125*, 625–636.
- (42) Yang, K.-L.; Yiacoumi, S.; Tsouris, C. Monte Carlo Simulations of Electrical Double-Layer Formation in Nanopores. *J. Chem. Phys.* **2002**, *117*, 8499–8507.
- (43) Hou, C.-H.; Taboada-Serrano, P.; Yiacoumi, S.; Tsouris, C. Monte Carlo Simulation of Electrical Double-Layer Formation from Mixtures of Electrolytes inside Nanopores. *J. Chem. Phys.* **2008**, *128*, No. 044705.
- (44) Qing, L.; Lei, J.; Zhao, T.; Qiu, G.; Ma, M.; Xu, Z.; Zhao, S. Effects of Kinetic Dielectric Decrement on Ion Diffusion and Capacitance in Electrochemical Systems. *Langmuir* **2020**, *36*, 4055–4064.
- (45) Mittal, J.; Errington, J. R.; Truskett, T. M. Thermodynamics Predicts How Confinement Modifies the Dynamics of the Equilibrium Hard-Sphere Fluid. *Phys. Rev. Lett.* **2006**, *96*, No. 177804.
- (46) Liu, Y. Development of 3-Dimensional Time-Dependent Density Functional Theory and Its Application to Gas Diffusion in Nanoporous Materials. *Phys. Chem. Chem. Phys.* **2016**, *18*, 13158–13163.
- (47) Babarao, R.; Jiang, J. Diffusion and Separation of CO₂ and CH₄ in Silicalite, C168 Schwarzite, and IRMOF-1: A Comparative Study from Molecular Dynamics Simulation. *Langmuir* **2008**, *24*, 5474–5484.
- (48) Beerdse, E.; Dubbeldam, D.; Smit, B. Understanding Diffusion in Nanoporous Materials. *Phys. Rev. Lett.* **2006**, *96*, No. 044501.
- (49) Jani, A.; Busch, M.; Mietner, J. B.; Ollivier, J.; Appel, M.; Frick, B.; Zanotti, J.-M.; Ghoufi, A.; Huber, P.; Fröba, M.; Morineau, D. Dynamics of Water Confined in Mesopores with Variable Surface Interaction. *J. Chem. Phys.* **2021**, *154*, No. 094505.
- (50) Schlaich, A.; Kappler, J.; Netz, R. R. Hydration Friction in Nanoconfinement: From Bulk via Interfacial to Dry Friction. *Nano Lett.* **2017**, *17*, 5969–5976.

Recommended by ACS

Advanced Three-Dimensional Microelectrode Architecture Design for High-Performance On-Chip Micro-Supercapacitors

Panpan Zhang, Xing Lu, *et al.*

NOVEMBER 11, 2022

ACS NANO

READ 

Flexible Solid Supercapacitors of Novel Nanostructured Electrodes Outperform Most Supercapacitors

Sangwon Cho, Yongsok Seo, *et al.*

OCTOBER 11, 2022

ACS OMEGA

READ 

Three-Dimensional, Submicron Porous Electrode with a Density Gradient to Enhance Charge Carrier Transport

Gayea Hyun, Seokwoo Jeon, *et al.*

JUNE 10, 2022

ACS NANO

READ 

Low-Tortuosity Thick Electrodes with Active Materials Gradient Design for Enhanced Energy Storage

Jingyi Wu, Guihua Yu, *et al.*

MARCH 02, 2022

ACS NANO

READ 

Get More Suggestions >